DOE/CE/23810-81

IMPACT OF AIR AND REFRIGERANT MALDISTRIBUTIONS ON THE PERFORMANCE OF FINNED-TUBE EVAPORATORS WITH R-22 AND R-407C

Final Report

Jangho Lee and Piotr A. Domanski

Building Environment Division
National Institute of Standards & Technology
U.S. Department of Commerce
Gaithersburg, Maryland 20899

July 1997

Prepared for
The Air-Conditioning and Refrigeration Technology Institute
Under
ARTI MCLR Project Number 665-54500

This research project is supported, in whole or in part, by U.S. Department of Energy grant number DE-FG02-1CE23810: Materials Compatibility and Lubricants Research (MCLR) on CFC-Refrigerant Substitutes. Federal funding supporting MCLR program constitutes 93.57% of allowable costs. Funding from non-government sources supporting the MCLR program consists of direct cost sharing of 6.43% of allowable costs; and in-kind contributions from the air-conditioning and refrigeration industry.

DISCLAIMER

The U.S. Department of Energy's and the air-conditioning industry's support for the Materials Compatibility and Lubricants Research (MCLR) program does not constitute an endorsement by the U.S. Department of Energy, nor by the air-conditioning and refrigeration industry, or the views expressed herein.

This work was performed under a Cooperative Research and Development Agreement between NIST and ARTI. Under the terms of the CRADA, this document may not be used as advertising for any product or service, nor may ARTI imply to anyone that the CRADA or the research results are an endorsement by NIST of any ARTI products or services.

ABSTRACT

The report presents basic features of the evaporator model, EVAP5M, and simulation results for an evaporator operating with R-22 and R-407C at non-uniform air and refrigerant distributions. EVAP5M was developed under this project to provide a tool for simulating a finned-tube air-to refrigerant evaporator operating with single-component refrigerants and refrigerant mixtures. The tube-by-tube modeling approach allowed for one-dimensional non-uniformity in the air velocity profile and arbitrary maldistribution on the refrigerant side. The model uses the Carnahan-Starling-DeSantis equation of state for calculating refrigerant thermodynamic properties.

Simulations were performed for three evaporator slabs with different refrigerant circuitry designs. For the maldistributions studied, maldistributed air caused much more significant capacity degradation than maldistributed refrigerant. In some cases capacity decreased to as low as 57 percent of the value obtained for uniform velocity profile. Simulation results showed that R-22 and R-407C have similar susceptibility to capacity degradation. Relative change of capacity varied depending on the evaporator design and maldistribution studied.

ACKNOWLEDGMENT

The authors thank Nicos Martys of NIST for performing finite-difference method simulations for this study. Acknowledgment is also due to ARTI Project Manager, Glenn Hourahan, and to the members of the Project Monitoring Committee, Charles Bullock, John Judge, Alexander Lim, Wayne Reedy, Raymond Rite, and Leonard Van Essen, who assisted in formulating the direction of the project.

TABLE OF CONTENTS

LIST OF TABLES

LIST OF FIGURES

NOMENCLATURE

A_o = air-side surface area
A_f = finned surface area
A_{pm} = pipe mean surface area
A_{po} = pipe outside surface area
C_{pa} = specific heat at constant pressure for air
FDM = finite-difference method
F_i = m_i/m_{total}, fraction of total refrigerant mass flow rate flowing through i^{th} circuit
G_i = refrigerant mass flux for i^{th} circuitry branch
i_{fgw} = latent heat of water
Le = $h_o/(h_D \cdot C_{pa})$, Lewis number
h.t.c. = heat-transfer coefficient
h_D = air-side mass transfer coefficient
h_i = inside-tube heat-transfer coefficient
h_l = heat-transfer coefficient for condensate (frost) layer
h_{tf} = heat-transfer coefficient for tube/fin contact
h_o = air-side heat transfer coefficient
K = material conductivity
L = center-to-center distance between neighboring tubes
m = mass flow rate
NTU = number of thermal units
P = pressure
Q_a = heat-transfer rate for a given tube on the air side
Q_f = heat-transfer rate from neighboring tube(s) through fins
Q_r = heat-transfer rate for a given tube on refrigerant side
RATIO = coil capacity at given refrigerant and air distributions divided by coil capacity at uniform distributions with the same refrigerant
R_i, R_j = resistance to flow offered by a given branch leaving a split point (it accounts for the effects of tube geometry, fluid density and viscosity)
S = shape factor
T = temperature
t_f = fin thickness
UA = heat-transfer conductance
W = assumed width of fin used for tube-to-tube heat transfer
X_p = thickness of the tube wall

α = $i_{fgw}(\omega_a - \omega_w)/(C_{pa}(T_a - T_w))$
ε = heat-transfer effectiveness
ϕ = fin efficiency
ω_{ai} = humidity ratio of air at tube inlet
ω_{ao} = humidity ratio of air at tube outlet
ω_{fm} = humidity ratio of saturated air at mean temperature of condensate wetting the fin
ω_w = humidity ratio of saturated air at temperature of condensate wetting the tube

Subscripts:

a = air
d-p = dew-point, at evaporator outlet
f = fin
i = inlet or i^{th}
l = latent
o = outlet or outside (air-side)
p = tube
r = refrigerant
s = sensible
sat = saturation
sup = superheat
tot = total
w = water or tube wall

INTRODUCTION

The zeotrope R-407C (R-32/125/134a (23/25/52)) has been identified as an alternative to R-22 for residential application. Because of its selection, this ternary mixture has been studied extensively in recent years, and many aspects of R-407C performance have been explained. However, it is still unknown what effects air-side and refrigerant-side maldistribution may have on the coil capacity if this zeotropic mixture is employed. The goal of this study was to provide this information. From a practical point of view, it is important to know whether refrigerant and air maldistributions affect the evaporator performance of R-407C to the same degree as the evaporator performance of R-22.

Although laboratory evaluation of equipment performance is generally preferable, this study would be extremely tedious, time consuming, and expensive if the laboratory option was chosen. On the other hand, the goal of this study could be reached via simulations since the relative performance of an evaporator is of interest, and a detailed simulation model can predict relative trends reasonably well. With this in mind, a previously developed tube-by-tube evaporator model, EVSIM [1,2], was selected as the starting point of this study. EVSIM can simulate performance of single-component refrigerants and was verified in a laboratory for an R-22 evaporator exposed to non-uniform velocity profiles. Under the project described here, EVSIM was upgraded to simulate refrigerant mixtures. The acronym of the upgraded model is EVAP5M.

Because of the complexity of the tube-by-tube model, the development of EVAP5M was a major effort and is described in the first part of this report. The second part presents information on simulations performed on three evaporator coils. The appendix contains a user's manual for the model.

DESCRIPTION OF THE EVAPORATOR MODEL

The evaporator model developed and used in this study, EVAP5M, has the capability to simulate performance of a finned-tube evaporator with one-dimensionally maldistributed air at the inlet. Figure 1 shows an example of a refrigerant circuit and velocity profile which may be simulated in the model. EVAP5M has its origin in EVSIM [1,2], an evaporator model developed for R-22 and other single-component refrigerants. The main development effort of EVAP5M was the upgrading of EVSIM so it could simulate zeotropic refrigerant mixtures. This effort included incorporating the Carnahan-Starling-DeSantis equation of state and introducing several new algorithms to allow calculations of heat transfer and pressure drop for zeotropic mixtures. The fundamental aspects of EVAP5M are the same as those of EVSIM. These are briefly described below, but can be reviewed in detail in [1,2].

Modeling Approach

The EVAP5M modeling scheme uses the tube-by-tube approach. The program recognizes each tube as a separate entity for which it calculates heat transfer. These calculations are based on inlet refrigerant and air parameters, properties, and mass flow rates. Evaporator simulation starts with the inlet refrigerant tubes and proceeds, tube by tube, along the refrigerant path. Tubes located in the first depth row are exposed to the same inlet air temperature, but the inlet air temperature for any of the remaining tubes depends on the heat transferred from the tubes located on the air path upstream a given tube. At the outset of simulation, air temperature is only known for the tubes in the first depth row and has to be estimated for other tubes. The model updates these estimates later during simulation. A successful run requires several passes through the refrigerant circuitry, tube-by-tube, each time updating inlet air and refrigerant parameters for each tube. EVAP5M completes a simulation when coil capacities calculated from two subsequent loops are within the imposed convergence parameter.

Heat and Mass Transfer Algorithms

Heat transfer calculations start with calculating the heat-transfer effectiveness, ε, for a given tube by one of the available relations [3].

$$\varepsilon \sim f\left(\mathrm{NTU} = \frac{UA}{C_{pa} m_a}\right) \tag{1}$$

With air temperature changing during heat transfer, the selection of the appropriate ε -NTU relation used depends on whether the refrigerant undergoes a temperature change during heat transfer. Once ε is determined, heat transfer from air to refrigerant is obtained using equation (2).

$$Q_a = m_a C_{pa} (T_{ai} - T_{ri}) \varepsilon \tag{2}$$

The overall heat-transfer coefficient, U, for a dry or wet finned tube is calculated by equation (3) which sums up the individual heat-transfer resistances between the refrigerant and the air.

$$U = \left(\frac{A_o}{h_i A_{pi}} + \frac{A_o X_p}{A_{pm} K_p} + \frac{1}{h_i} + \frac{A_o}{A_{po} h_{tf}} + \frac{1}{h_o (1+\alpha)\left(1 - \frac{A_f}{A_o}\left(1 - \phi_f\right)\right)} \right)^{-1} \tag{3}$$

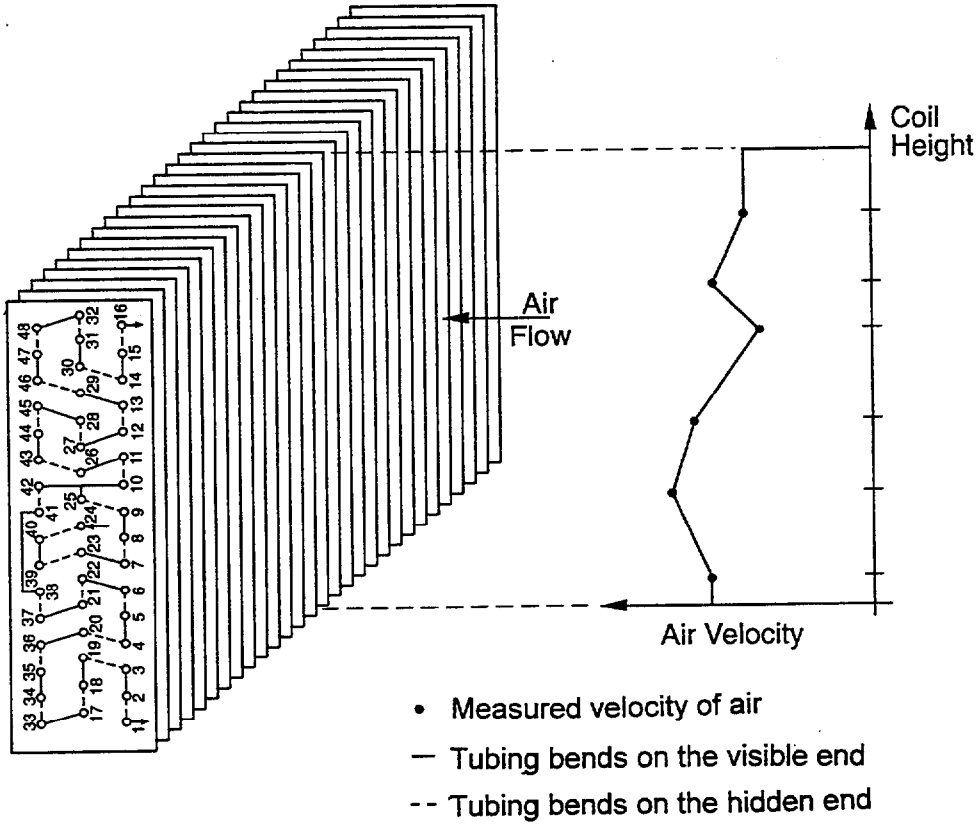

Figure 1. Schematic of refrigerant circuit and representation of air velocity profile

where

$$\alpha = \frac{i_{fgw}(\omega_a - \omega_w)}{C_{pa}(T_a - T_w)} \tag{4}$$

The first and the fifth terms of equation (3) represent the refrigerant-side and air-side convection resistances, respectively. The second term is the conductive heat-transfer resistance through the tube wall, and the third term accounts for the conduction resistance through the water layer on the fin and tube. The fourth term represents the contact resistance between the outside tube surface and the fin collar. The fifth term is the conduction resistance on the air side where the multiplier (1+α) in the denominator accounts for the latent heat transfer on the outside surface. For a dry tube $\alpha = 0.0$ and $1/h_i = 0.0$.

Once the heat transfer rate from air to refrigerant is calculated, the tube wall temperature and the fin surface temperature can be calculated directly using heat-transfer resistances. Then, humidity ratios for the saturated air at the wall and fin temperatures are calculated, and mass transfer from the air to the tube and fin surfaces is determined from equation (5).

$$\Delta\omega = (\omega_{ai} - \omega_w)\left(1 - \exp\left(\frac{-h_o A_{po}}{\mathrm{Le} C_{pa} m_a}\right)\right) + (\omega_{ai} - \omega_{fm})\left(1 - \exp\left(\frac{-h_o A_f}{\mathrm{Le} C_{pa} m_a}\right)\right) \tag{5}$$

The first term in equation (5) calculates mass transfer from the air to the tube wall, and the second term calculates the mass transfer from the air to the fin surface. The Lewis number, Le, is assumed to be equal to 1.0. The model uses the same air-side heat-transfer coefficient for both tube and fin surfaces. The calculation scheme is of iterative nature. The properties that are unknown at the outset of simulation are initially estimated, and later the estimated values are replaced with the values obtained in the previous iteration loop.

After $\Delta\omega$ is determined, the outlet air humidity ratio and temperature for a given tube are evaluated by equations (6) and (7).

$$\omega_{ao} = \omega_{ai} - \Delta\omega \tag{6}$$

$$T_{ao} = T_{ai} - \frac{Q_a}{m_a C_{pa}} + \frac{i_{fgw}\Delta\omega}{C_{pa}} \tag{7}$$

Since tubes are usually arranged in a staggered pattern, the program uses the outlet temperatures and humidity ratios for the two closest upstream neighbors to calculate the inlet air parameters for a tube in the second and farther depth row. A mixing rule (0.5/0.5) is applied.

Refrigerant Distribution

In a heat exchanger with multiple circuits, refrigerant distributes itself in appropriate proportions so refrigerant pressure drop in all circuits from inlet to outlet is the same. Equation (8) uses the same principle to calculate a fraction of the total refrigerant mass flow rate flowing through a particular circuit.

$$F_i = \frac{m_i}{m_{total}} = \sum_{j=first}^{last} \left[\frac{1}{\left(R_i / R_j\right)^{0.571}} \right] \tag{8}$$

where $R_i = \Delta P_i / \Delta G_i^{1.75}$ is the flow resistance for a given circuitry branch for which F_i is calculated, and $R_j = \Delta P_j / \Delta G_j^{1.75}$ represents the flow resistance for each circuitry branch meeting in a given split point (j=first to last circuitry branch). Equation (8) was derived in reference [1] for the Pierre pressure drop correlation and can only be used by evaporator simulation models using this correlation for calculating pressure drop.

At the outset of the calculation for the first iteration loop, the model estimates the (i)th circuit resistance, R_i, assuming the same flow resistance in each tube regardless of flow quality. Thus, the initial values of R_i depend on the number of tubes in a given circuit and the circuit's layout (circuit split points and their location). For subsequent iterations, the values of R_i and F_i are updated using the pressure drops calculated in the previous simulation loop. In the course of simulation, refrigerant distribution is updated and ΔP_j become identical (within a convergence parameter).

Improvements in EVAP5M over EVSIM

EVAP5M has its origin in EVSIM [1,2] and is based on the same general concepts. However, these two models differ due to several new algorithms introduced to EVAP5M. The modifications made include:

- employing REFPROP Version 5 [4] routines for calculating thermodynamic and transport properties
- adding a heat-transfer relation for calculating heat-transfer between a two-phase zeotropic refrigerant mixture and air
- introducing new heat-transfer and pressure drop correlations
- improving the calculation scheme for determining mixed air properties for the second and farther tube depth rows
- adding an algorithm to account for the heat conduction between tubes through fins. (This item offered the most conceptual difficulty and is described in some detail in a separate section below.)

In the process of making these modifications, the program was carefully screened in the debugging mode using two different compilers. These procedures allowed the identification and removal of several hidden code errors and improved the robustness of the program.

Heat Conduction Between Tubes through Fins

EVAP5M calculates the heat transfer between tubes independently from calculations of the heat transfer between refrigerant and air; that is, EVAP5M calculates the refrigerant-to-air heat transfer first and then corrects the total refrigerant heat gain (or loss) in a given tube for the amount of heat transferred by fins. This calculation scheme is expressed by equation (9).

$$(Q_r)_j^i = (Q_a)_j^i + (\sum_n (Q_f)_n)_j^{i-1} \tag{9}$$

The first term represents the heat transferred between the tube and the air, and the second term with a summation mark represents the heat transferred via fins between the analyzed tube and other tubes in the slab. Calculating heat transfer between tubes requires the knowledge of temperature for each tube. Since at the outset of calculations (first iteration loop) tube temperatures are unknown, evaluation of fin conduction effects starts with the second iteration

loop using tube temperatures calculated in the previous loop. Thus, index j is the identification number for the analyzed tube, indices i and i-1 denote the current and previous iteration loops, respectively, and index n stands for the number of neighboring tubes that exchange heat with tube j. The summation of the second term of equation (9) for all tubes is zero because fin conduction heat transfer is an internal process in a given evaporator.

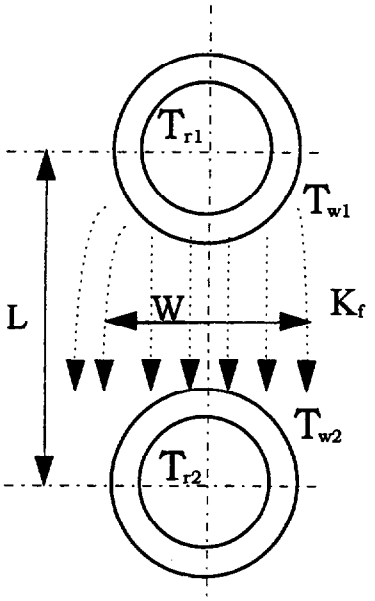

Figure 2. Schematic graph for fin heat conduction between two adjacent tubes

Sheffield [11] applied a shape factor, S, to determine the fin heat conduction resistance between a hot collar and a cold collar, as presented in Figure 2 and equation (10).

$$(Q_{fin})_{12} = \left(\frac{W \cdot t_f}{L} K_f\right)(T_{w1} - T_{w2}) = S \cdot t_f \cdot K_f (T_{w1} - T_{w2}) \tag{10}$$

The value of the shape factor will depend on a fin design. For flat and wavy fins the fin material is continuous. Louvered fins, however, have numerous cuts, which reduce the fin cross-section area available for heat transfer. The authors are not aware of any publication that quantifies the shape factor. In this situation, they decided to use the outer-diameter of the tube, D_o, as the basis for defining S and to adopt the following values: D_o for flat and wavy fins, 0.7 D_o for lanced fins, and 0.5D_o for louvered fins. Note, that different values for the shape factor may be justified within a given class (lanced or louvered) because of a different number of cuts and their configuration in different designs.

A given tube in an evaporator can have a minimum of two neighboring tubes and a maximum of six neighboring tubes. For the convenience of calculation, EVAP5M considers conduction heat transfer only between these immediate neighboring tubes although some heat transfer may take place between more distant tubes. The adequacy of this simplification was validated with a finite-difference method (FDM) algorithm which was used to solve a heat diffusion equation [5] accounting for heat conduction between all tubes in the coil assembly.

Figure 3 shows a schematic side view of the evaporator used for the validation. The tube temperatures shown in the figure were obtained from EVAP5M simulations. These temperatures

were used as input to the FDM. Figure 4 presents the net heat gains or heat losses for each tube calculated by both methods. The results can be intuitively confirmed with the tube temperatures shown in Figure 3. The tubes with a superheated vapor lose heat to the second-row tubes. Tube # 1 has the highest heat loss because it has the highest temperature. Tube # 4 has the smallest heat transfer because the heat gain from tube # 3 is offset by the heat loss to tube # 5. Tubes # 9, # 10, # 11, and # 12 have similar heat gains from the tubes in the middle depth row. The results from EVAP5M are similar in both trend and magnitude to those obtained with the FDM algorithm. The agreement between the EVAP5M and FDM results justifies using the simplified approach in the evaporator model. Note that heat transfer between tubes via fins is affected by the air-side heat transfer coefficient. A rigorous evaluation of this effect would require a separate project dedicated to studying this influence.

The tube-to-tube heat transfer depends on the temperature difference between neighboring tubes and will vary between different refrigerant circuit designs, refrigerants, and operating conditions (refrigerant superheat and drop of saturation temperature due to pressure drop). If a given tube and its neighbors contain a two-phase refrigerant, the heat transferred between the tube and its neighbors will be an infinitesimal fraction of the heat transferred between the tube and the air stream. However, if a tube contains a superheated refrigerant with its temperature approaching that of the air and the neighboring tubes contain a two-phase refrigerant, the tube-to-tube heat transfer may be a significant part of the total heat transfer for this tube.

To assess the model sensitivity to the tube-to-tube heat-transfer algorithm, selected simulations were performed with a flag setting that disabled the tube-to-tube heat-transfer scheme. The difference in simulated coil capacity obtained with and without tube-to-tube heat transfer varied between the cases studied. The simulated capacity was as much as 5 percent greater when tube-to-tube heat transfer was not considered.

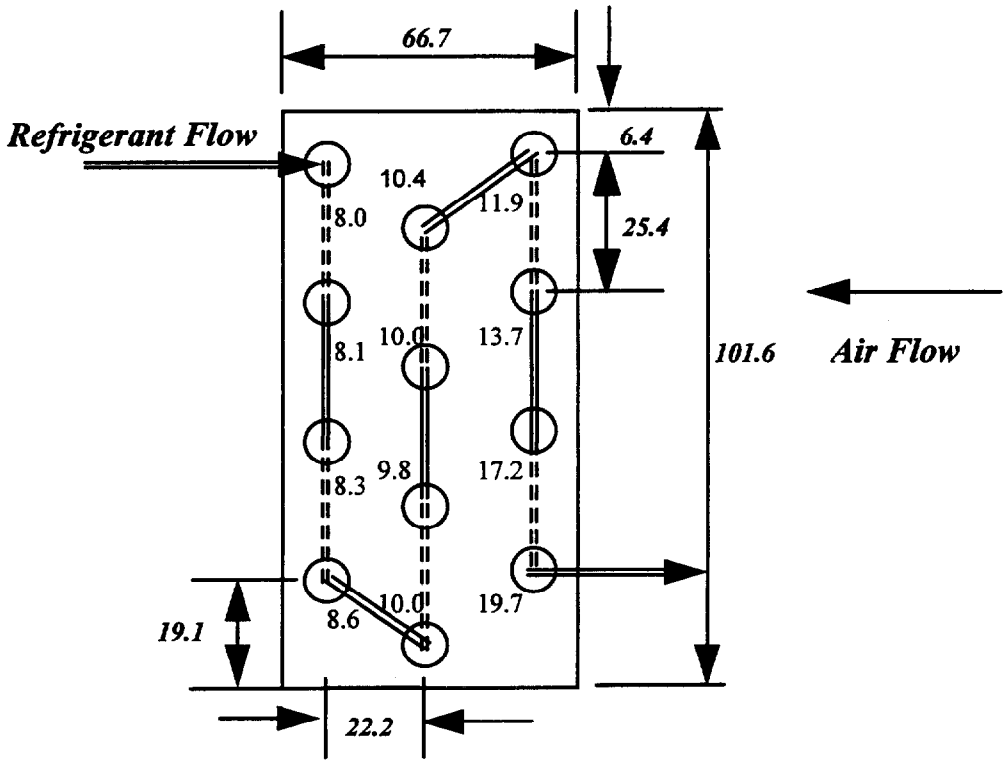

Figure 3. Side dimensions (mm) of the evaporator and tube temperatures (°C) used for fin heat conduction calculations (side dimensions are shown in bold italic)

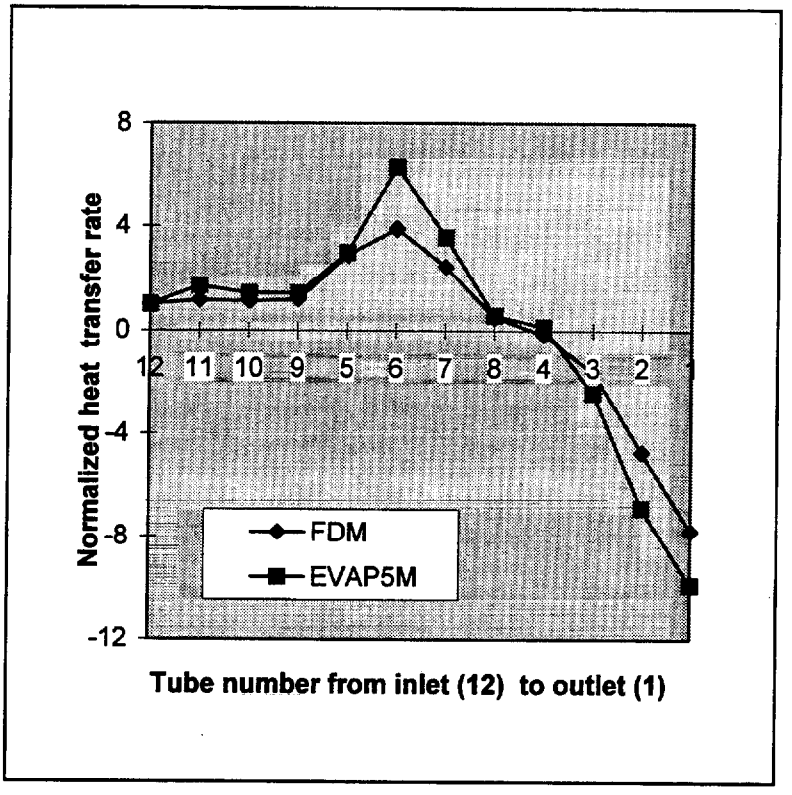

Figure 4. Normalized conduction heat transfer rate calculated by EVAP5M and FDM (Heat transfer rate for a given tube divided by heat transfer rate for the inlet tube (# 12))

Heat Transfer and Pressure Drop Correlations

EVAP5M uses the following correlations for calculating heat transfer and pressure drop.

Air Side

- heat-transfer coefficient for flat fins: Gray/ Webb [6]
- heat-transfer coefficient for wavy fins: Webb [7]
- heat-transfer coefficient for lanced fins: Nakayama/Xu [8]
- fin efficiency: Schmidt method, described in [9]
- heat-transfer coefficient for tube/fin collar junction: Sheffield et al. [10]

Refrigerant Side

- single-phase heat-transfer coefficient, smooth tube: McAdams, described in [11]
- evaporation heat-transfer coefficient up to 80% quality, smooth tube: Jung/Didion [12]
- mist flow, smooth and rifled tubes: linear interpolation between h.t.c. values for 80% and 100% quality
- single-phase pressure drop, smooth tube: Petukhov [13]
- two-phase pressure drop, smooth tube: Pierre [14]
- single-phase pressure drop, return bend, smooth tube: White, described in [15]
- two-phase pressure drop, return bend, smooth tube: Chisholm, described in [16]

Calculations of the air-side heat-transfer coefficient for wavy and lanced fins employ the flat fin correlation [6] for obtaining a reference h.t.c. value and use the correlations from references [7] and [8] for obtaining an enhancement multiplier. This relative evaluation of the air-side heat-

transfer is not of essence for this study because only lanced fins are considered, but it is beneficial for simulations where evaporators with flat, wavy, and lanced fins are compared. The Sheffield correlation for the tube-collar junction h.t.c. was included in the calculation scheme (equation 3) because 10 out of 16 heat exchangers used for the development of the Gray/Webb correlation were metallurgically bonded, which practically eliminates the fin-collar heat-transfer resistance. Only the remaining 6 coils were bonded by mechanical tube expansion and their air-side data included a typical heat-transfer resistance on the tube-collar junction.

On the refrigerant side, the heat-transfer coefficient for a rifled tube was calculated by applying a 1.9 multiplier to the value of the heat-transfer coefficient calculated for a smooth tube [17]. For calculating a pressure drop in a rifled tube, EVAP5M used the smooth tube pressure drop and a multiplier of 1.4 [17].

Model Verification

References [1] and [2] report R-22 evaporator capacities measured at four different velocity profiles. The tests were run at operating conditions typical for a residential system evaporator ($T_{sat} \cong$ 7.1 °C). Different velocity profiles were obtained by installing the evaporator at different angles in the air duct. These test data were used in [1,2] to validate EVSIM and were also applied in the current study to validate EVAP5M. Table 1, Figure 5 and Figure 6 present the test results and simulation results from EVSIM and EVAP5M. For total capacity, the EVAP5M predictions are lower than the EVSIM predictions and the test data. However, the capacity trend predicted by EVAP5M agrees better with the tested capacity than that of EVSIM. A better agreement in absolute values between the test and EVAP5M results could be attained by tuning heat transfer coefficients on the refrigerant and air side. This was not carried out since this study is concerned with relative evaluation of capacity (capacity degradation), and a better agreement in absolute results is not essential.

In general, latent capacity results also follow the trend of the test data but with a considerable scatter. Note, that EVAP5M first calculates the total and then the latent evaporator capacity as a fraction of the total capacity. This explains why the total capacity trend is smooth regardless of scattered predictions for the latent capacity.

Table 1. Test and simulation results for one evaporator with four velocity profiles

Velocity[1] profile	Total Capacity				Latent Capacity			
	Test (kW)	EVSIM (kW)	EVAP5M (kW)	Discrepancy[2] (%)	Test (kW)	EVSIM (kW)	EVAP5M (kW)	Discrepancy[2] (%)
DTEV25	4.365	4.354	4.079	-6.56	1.213	1.364	1.066	-12.10
DTEV45	4.859	4.518	4.307	-11.36	1.399	1.668	1.367	-2.30
DTEV65	5.206	4.780	4.611	-11.43	1.493	1.371	1.151	-22.89
DTEV90	5.416	5.092	4.865	-10.17	1.555	1.472	1.448	-6.87

[1] Test data and velocity profile designation taken from reference [1]. The number in the velocity profile designation represents the angle of approach.
[2] 100% · (EVAP5M Value -Test Value) / Test Value

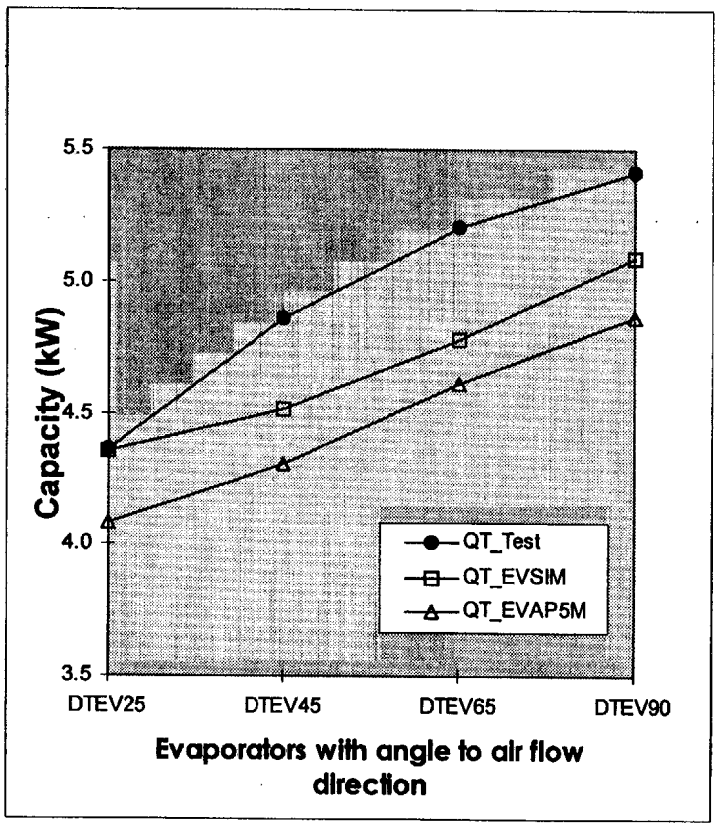

Figure 5. Total capacity by test and simulations

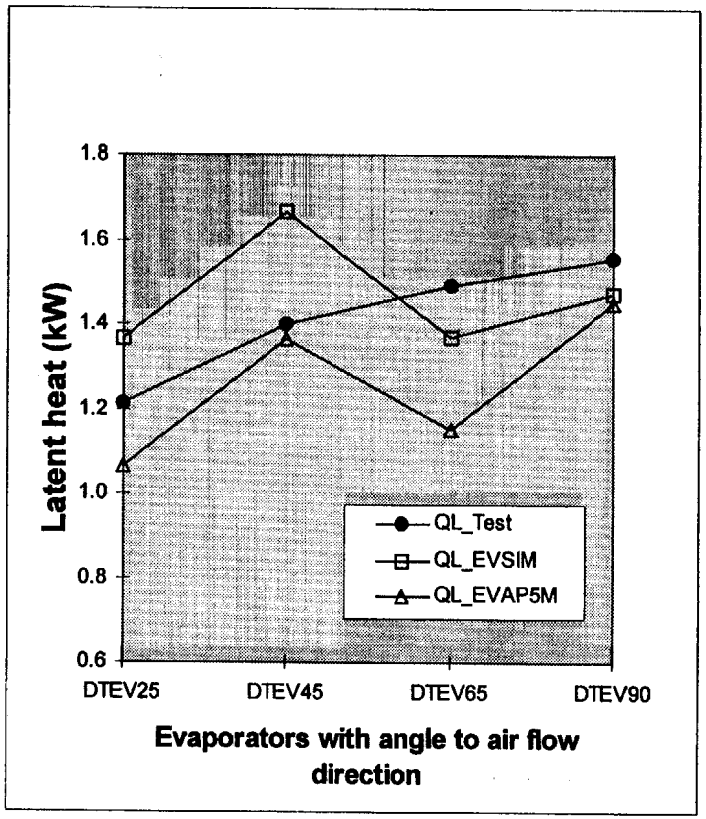

Figure 6. Latent heat transfer by test and simulations

SIGNIFICANT RESULTS

Simulated Evaporators and Simulation Conditions

This study considered three evaporators. For clarity of discussion, the evaporators had identical design specifications but different refrigerant circuitry. Each heat exchanger had six refrigerant circuits with six tubes per circuit, but the arrangement of refrigerant flow was different for each coil. The evaporator designs (including refrigerant circuits) and air velocity profiles were specified by the Project Monitoring Committee. In this report, the three evaporators are denoted as Coil A, Coil B, and Coil C.

Table 2 contains design data, and Figures 7 and 8 schematically show the side views of the coils and the velocity profiles applied. In these figures, the circles denote refrigerant tubes, while the lines connecting the centers of some of the circles represent the visible return bends. The returning bends on the hidden end are dotted. All six refrigerant circuits in Coil A are identical and have a counter-cross flow arrangement. For Coil B, all refrigerant circuits are also identical, but they have a counter-cross-parallel arrangement. Coil C may be considered to be an assembly of two identical sections positioned one on another, each with three circuits. The circuit having the refrigerant inlet in the first depth row (facing the incoming air) uses three tubes in the first row and then crosses over to the third row, where refrigerant flows through the remaining three tubes and leaves the coil. The circuit with the inlet in the second depth row has all six tubes in the same row. The third circuit is symmetrical to the first circuit; it starts in the third depth row and ends in the first row.

Table 2.. Evaporator specification

Item	Data	
Number of tube depth rows	3	
Number of tubes per depth row	12	
Tube inner diameter	9.20 mm	(0.362 in)
Tube outer diameter	9.91 mm	(0.390 in)
Tube pitch in the same depth row	25.40 mm	(1.00 in)
Depth row pitch	22.00mm	(0.866 in)
Coil width (finned tube length)	914.4 mm	(36.0 in)
Coil face area	0.28 m^2	(3.0 ft^2)
Fin pitch	1.81 mm	(0.071 in)
Fin thickness	0.14mm	(0.0055 in)
Fin thermal conductivity	0.219 kW/(m °C)	(126.5 Btu/(ft·h·°F))
Tube thermal conductivity	0.339 kW/(m °C)	(195.5 Btu/(ft·h·°F))
Type of fin	lanced	
Type of in-tube enhancement	rifled	

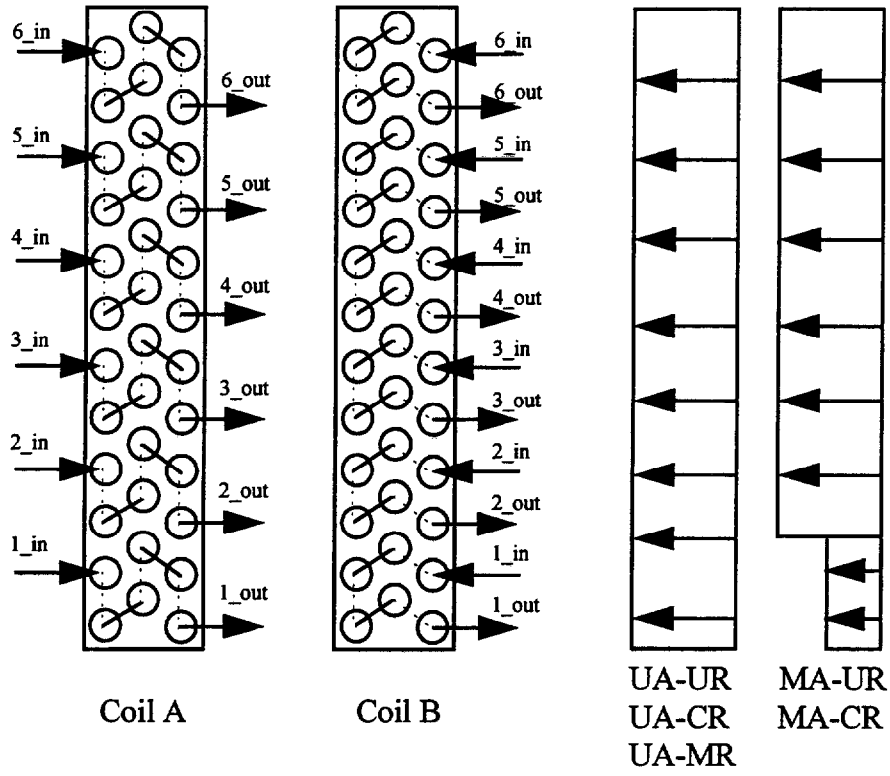

Figure 7. Refrigerant circuitry arrangement and air velocity profiles for Coil A and Coil B

Figure 7 includes the uniform and maldistributed velocity profiles simulated with Coil A and Coil B. These velocity profiles were used in combination with three refrigerant distributions, as listed in Table 3. The maldistributed and uniform refrigerant distributions were imposed as input. In the cases with calculated refrigerant distribution (CR), the refrigerant distribution was assigned by the model based on the pressure drop calculated for individual circuits. The designation scheme for different combinations of air and refrigerant distributions uses the letter U for uniform, M for maldistributed, C for calculated (simulated), and A and R for air and refrigerant, respectively.

Figure 8 explains simulations performed for Coil C. They included a case with the uniform refrigerant distribution and uniform air (UA-UR) and four cases with the shown air velocity profiles and simulated refrigerant distribution. For the simulation cases denoted by MA1-CR and MA2-CR, the lowest air velocity (at the edge of the coil) was equal to 66% and 33% of the average air velocity, respectively.

This study considered each coil as a separate case, but simulations were carried out according to the same procedure using several common parameters. The constant parameters for any simulation were:

- air inlet dry-bulb temperature: 26.7 °C (80.0 °F)
- air inlet wet-bulb temperature: 19.4 °C (67.0 °F)
- air volumetric flow rate: 27.0 m^3/min (953.0 ft^3/min)
- air face velocity: 96.4 m/min (317.7 ft/min)
- refrigerant inlet quality: 0.20
- refrigerant superheat at coil outlet: 4.4 °C (8.0 °F)

Simulation runs with R-22 for uniform air and refrigerant distributions (UA-UR) served as the starting point for each coil. These simulations were performed for 7.8 °C (46.0 °F) refrigerant saturation temperature and 4.4 °C (8.0 °F) superheat at the evaporator outlet. This required repetitive runs to iterate refrigerant inlet pressure and refrigerant mass flow rate. Subsequent simulations with R-22 used the same refrigerant inlet pressure but iterated refrigerant mass flow rate to obtain the target superheat of 4.4 °C (8.0 °F).

Table 3. Simulation cases for Coil A and Coil B

No.	Case	Air	Refrigerant
1	UA-UR	Uniform	Uniform
2	UA-CR	Uniform	Calculated
3	UA-MR	Uniform	17.24% for 5 circuits 13.80% for 1 circuit
4	MA-UR	18.17% for 5 circuits 9.15% for 1 circuit	Uniform
5	MA-CR	18.17% for 5 circuits 9.15% for 1 circuit	Calculated

The R-22 capacity from the UA-UR run was used as the target capacity for the UA-UR run with R-407C. For the R-407C UA-UR simulation, refrigerant inlet pressure and refrigerant mass flow rate were iterated to obtain the target capacity and superheat of 4. 4. °C (8.0 °F). The resulting refrigerant inlet pressure that provided the capacity match was used in subsequent R-407C simulations at non-uniform air or refrigerant distributions. As in R-22 runs, the target refrigerant superheat of 4.4 °C (8.0 °F) was obtained by iterating refrigerant mass flow rate. The conversion criteria in the performed iterations were 0.2% of total enthalpy difference, 0.1% of total pressure drop, and ±0.3 °C (0.5 °F) of refrigerant superheat.

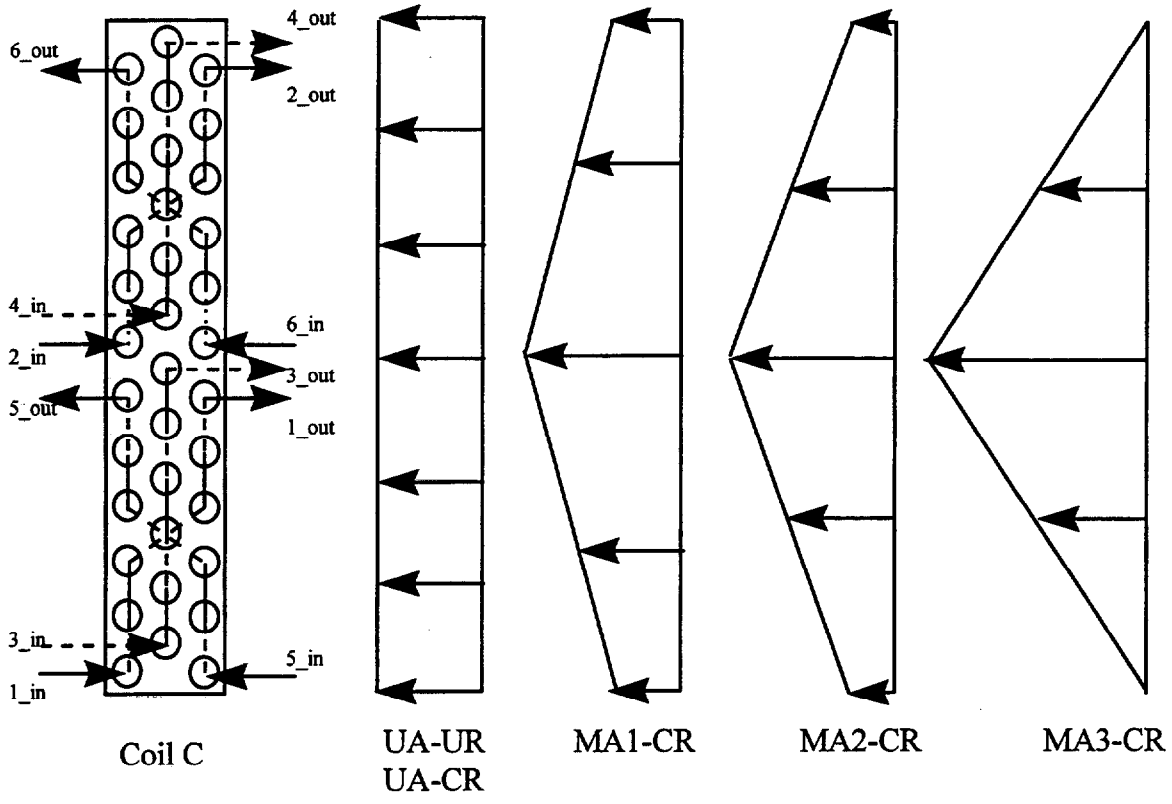

Figure 8. Refrigerant circuitry arrangement and air velocity profiles for Coil C

Simulation Results

Table 4 shows a summary of simulation results. The table includes refrigerant mass flow rates, evaporator inlet and outlet pressures, and saturation temperatures and superheats at the evaporator outlet. The last column contains a ratio of capacity at given air and refrigerant distributions to the capacity obtained for uniform distributions of refrigerant and air. This ratio is a measure of capacity reduction due to maldistributed flows. Table 5 provides additional information on refrigerant distribution, outlet quality and superheat for individual evaporator circuits. The sections below discuss the obtained results individually for each evaporator.

Table 4. Simulation results

No.	Coil	Simulation	Refrig.	m_r kg/h	P_{inlet} kPa	T_{inlet} °C	P_{outlet} kPa	T_{d-p} °C	T_{sup} °C	Q_s kW	Q_l kW	Q_{tot} kW	Ratio
1	A	UA-UR	R-22	222.8	645.1	8.2	636.7	7.8	4.4	6.79	3.29	10.08	1.00
2	A	UA-CR	R-22	212.3	645.4	8.2	636.7	7.8	4.4	6.59	3.01	9.60	0.95
3	A	UA-MR	R-22	221.1	645.3	8.2	636.7	7.8	4.4	6.90	3.10	10.00	0.99
4	A	MA-UR	R-22	203.2	645.2	8.2	636.7	7.8	4.5	5.99	3.21	9.20	0.91
5	A	MA-CR	R-22	135.9	645.1	8.2	636.7	7.8	4.4	4.21	1.94	6.15	0.61
6	A	UA-UR	R-407C	210.7	652.5	5.4	645.1	10.1	4.5	6.51	3.57	10.08	1.00
7	A	UA-CR	R-407C	210.5	652.6	5.4	645.2	10.1	4.5	6.51	3.56	10.07	1.00
8	A	UA-MR	R-407C	208.7	652.5	5.4	645.1	10.1	4.5	6.54	3.44	9.98	0.99
9	A	MA-UR	R-407C	191.7	651.9	5.4	645.1	10.1	4.5	5.74	3.43	9.17	0.91
10	A	MA-CR	R-407C	163.1	650.3	5.3	645.1	10.1	4.5	4.99	2.82	7.81	0.77
11	B	UA-UR	R-22	225.1	646.2	8.3	636.7	7.8	4.5	6.73	3.45	10.18	1.00
12	B	UA-CR	R-22	211.6	646.4	8.3	636.7	7.8	4.4	6.68	2.88	9.57	0.94
13	B	UA-MR	R-22	220.5	646.2	8.3	636.7	7.8	4.5	6.88	3.09	9.97	0.98
14	B	MA-UR	R-22	204.2	646.4	8.3	636.7	7.8	4.5	5.66	3.28	8.94	0.88
15	B	MA-CR	R-22	147.1	643.3	8.1	636.7	7.8	4.4	4.93	1.73	6.66	0.65
16	B	UA-UR	R-407C	212.5	642.3	4.9	634.2	9.6	4.4	6.77	3.42	10.18	1.00
17	B	UA-CR	R-407C	210.7	642.3	4.9	634.2	9.6	4.4	6.82	3.23	10.06	0.99
18	B	UA-MR	R-407C	206.9	642.1	4.9	634.2	9.6	4.5	6.85	3.07	9.92	0.97
19	B	MA-UR	R-407C	187.3	641.4	4.9	634.2	9.6	4.4	6.01	2.97	8.98	0.88
20	B	MA-CR	R-407C	155.7	639.9	4.8	634.2	9.6	4.5	5.46	2.02	7.47	0.73
21	C	UA-UR	R-22	211.7	645.7	8.2	636.7	7.8	4.5	6.51	3.07	9.58	1.00
22	C	UA-CR	R-22	195.5	645.2	8.2	636.7	7.8	4.4	6.04	2.80	8.84	0.92
23	C	MA-1CR	R-22	144.0	640.0	8.0	636.7	7.8	4.4	5.41	1.12	6.53	0.68
24	C	MA-2CR	R-22	142.1	639.9	7.9	636.7	7.8	4.5	5.28	1.16	6.44	0.67
25	C	MA-3CR	R-22	134.6	639.7	7.9	636.7	7.8	4.5	4.92	1.18	6.10	0.64
26	C	UA-UR	R-407C	634.6	641.9	4.5	634.2	9.6	4.5	6.39	3.20	9.58	1.00
27	C	UA-CR	R-407C	195.9	641.7	4.6	634.7	9.6	4.4	6.30	3.09	9.39	0.98
28	C	MA-1CR	R-407C	116.9	636.7	4.6	634.6	9.6	4.5	4.72	0.89	5.62	0.59
29	C	MA-2CR	R-407C	116.0	636.7	4.6	634.6	9.6	4.4	4.65	0.92	5.57	0.58
30	C	MA-3CR	R-407C	113.5	636.6	4.6	634.6	9.6	4.5	4.45	1.00	5.45	0.57

Distribution designation: UA = uniform air
MA = maldistributed air
UR = uniform refrigerant (imposed)
MR = maldistributed refrigerant (imposed)
CR = calculated refrigerant

Table 5. Refrigerant mass flow rate fraction, outlet quality, and superheat for individual circuits

R-22

COIL	Condition	Item \ circuit no.	1	2	3	4	5	6
A	UA-UR	Ref. Flow	0.167	<----	<----	<----	<----	<----
		Outlet Quality	1.00	<----	<----	<----	<----	<----
		Super Heat	6.67	3.62	3.42	3.45	3.54	6.06
	UA-CR	Ref. Flow	0.148	0.142	0.177	0.194	0.188	0.152
		Outlet Quality	1	<----	<----	0.956	0.998	1
		Super Heat	15.3	13.69	5.8	0	0	11.48
	UA-MR	Ref. Flow	0.138	0.172	<----	<----	<----	<----
		Outlet Quality	1.00	<----	<----	<----	<----	<----
		Super Heat	15.4	8.83	0.89	0.46	0.57	2.71
	MA-UR	Ref. Flow	0.167	<----	<----	<----	<----	<----
		Outlet Quality	0.87	1	<----	<----	<----	<----
		Super Heat	0	10.76	12.66	12.92	12.8	14.77
	MA-CR	Ref. Flow	0.252	0.172	0.149	0.143	0.141	0.143
		Outlet Quality	0.88	1	<----	<----	<----	<----
		Super Heat	0	16.21	16.5	17.94	18.05	18.15
B	UA-UR	Ref. Flow	0.167	<----	<----	<----	<----	<----
		Outlet Quality	1	<----	<----	<----	<----	<----
		Super Heat	5.96	3.59	3.46	3.5	3.62	6.52
	UA-CR	Ref. Flow	0.147	0.195	0.194	0.165	0.145	0.153
		Outlet Quality	1	0.972	0.974	1	1	1
		Super Heat	15.08	0	0	10.32	11.94	11.22
	UA-MR	Ref. Flow	0.141	0.187	0.186	0.174	0.159	0.153
		Outlet Quality	1	<----	<----	<----	<----	<----
		Super Heat	15.26	2.58	2.02	2.11	2.22	4.75
	MA-UR	Ref. Flow	0.167	<----	<----	<----	<----	<----
		Outlet Quality	0.867	1	<----	<----	<----	<----
		Super Heat	0	11.5	12.6	12.61	12.5	14.4
	MA-CR	Ref. Flow	0.237	0.148	0.154	<----	<----	<----
		Outlet Quality	1	1	0.974	0.985	1	1
		Super Heat	0	16	0	0	16.01	16.03
C	UA-UR	Ref. Flow	0.167	<----	<----	<----	<----	<----
		Outlet Quality	1	1	0.977	1	1	1
		Super Heat	8.35	10.33	0	1.61	6.29	6.43
	UA-CR	Ref. Flow	0.184	0.172	0.2	0.167	0.139	0.139
		Outlet Quality	1	<----	0.953	1	<----	<----
		Super Heat	7.41	12.33	0	8.79	6.86	8.23
	MA1-CR	Ref. Flow	0.183	0.169	0.176	0.163	0.153	0.156
		Outlet Quality	1	<----	<----	<----	<----	<----
		Super Heat	2.36	6.04	1.47	3.63	6.28	7.29
	MA2-CR	Ref. Flow	0.181	0.172	0.178	0.155	0.158	0.155
		Outlet Quality	1	<----	<----	<----	<----	<----
		Super Heat	3.53	3.41	1.34	5.54	7.13	6.47
	MA3-CR	Ref. Flow	0.181	0.178	0.179	0.158	0.16	0.145
		Outlet Quality	1	<----	<----	<----	<----	<----
		Super Heat	5.11	0.00	2.72	5.14	8.54	5.85

R-407C

COIL	Condition	Item \ circuit no.	1	2	3	4	5	6
A	UA-UR	Ref. Flow	0.167	<----	<----	<----	<----	<----
		Outlet Quality	1.00	<----	<----	<----	<----	<----
		Super Heat	6.33	4.21	3.75	3.82	3.94	4.83
	UA-CR	Ref. Flow	0.160	0.169	0.17	0.169	0.169	0.164
		Outlet Quality	1	<----	<----	<----	<----	<----
		Super Heat	8.83	3.54	2.64	2.8	3.45	5.85
	UA-MR	Ref. Flow	0.138	0.172	<----	<----	<----	<----
		Outlet Quality	1	<----	<----	<----	<----	<----
		Super Heat	12.43	6.45	2.16	1.85	2.13	3.31
	MA-UR	Ref. Flow	0.167	<----	<----	<----	<----	<----
		Outlet Quality	0.925	1	<----	<----	<----	<----
		Super Heat	0	7.6	9.06	9.61	9.88	10.42
	MA-CR	Ref. Flow	0.205	0.156	0.158	0.157	0.158	0.165
		Outlet Quality	0.898	1	<----	<----	<----	<----
		Super Heat	0	9.73	12.34	12.94	12.94	13.38
B	UA-UR	Ref. Flow	0.167	<----	<----	<----	<----	<----
		Outlet Quality	1	<----	<----	<----	<----	<----
		Super Heat	7.31	3.96	3.65	3.67	3.85	4.27
	UA-CR	Ref. Flow	0.156	0.17	<----	<----	0.168	0.165
		Outlet Quality	1	<----	<----	<----	<----	<----
		Super Heat	9.77	3.41	2.72	2.86	3.9	4.44
	UA-MR	Ref. Flow	0.138	0.172	<----	<----	<----	<----
		Outlet Quality	1	<----	<----	<----	<----	<----
		Super Heat	13.09	3.61	2.67	2.69	2.83	3.55
	MA-UR	Ref. Flow	0.167	<----	<----	<----	<----	<----
		Outlet Quality	0.956	1	<----	<----	<----	<----
		Super Heat	0	7.49	8.24	8.27	8.27	8.06
	MA-CR	Ref. Flow	0.204	0.161	0.158	0.158	0.158	0.16
		Outlet Quality	0.944	1	<----	<----	<----	<----
		Super Heat	0	9.73	9.89	9.91	9.9	9.77
C	UA-UR	Ref. Flow	0.167	<----	<----	<----	<----	<----
		Outlet Quality	1	<----	<----	<----	<----	<----
		Super Heat	6.52	9.34	0	3.59	3.16	4.41
	UA-CR	Ref. Flow	0.172	0.168	0.178	0.166	0.154	0.162
		Outlet Quality	1	<----	0.991	1	<----	<----
		Super Heat	5.71	10.1	0	4.26	4.4	5.79
	MA1-CR	Ref. Flow	0.172	0.163	0.17	0.16	0.166	0.169
		Outlet Quality	1	<----	<----	<----	<----	<----
		Super Heat	3.57	8.4	1.46	4.46	1.29	7.49
	MA2-CR	Ref. Flow	0.174	0.161	0.171	0.16	0.166	0.168
		Outlet Quality	1	<----	<----	<----	<----	<----
		Super Heat	3.76	7.82	1.78	4.47	1.67	7.28
	MA3-CR	Ref. Flow	0.175	0.159	0.17	0.166	0.163	0.168
		Outlet Quality	1	<----	<----	<----	<----	<----
		Super Heat	4.59	5.83	2.77	6.32	2.91	4.32

<---- indicates that the number is the same as for the column on the left hand side

Results for Coil A (cross-counter flow circuitry arrangement)

Figure 9 and positions 1 through 10 in Table 4 show relative capacity change for Coil A. The first three cases in the figure (entries 1 through 3 and 6 through 8 in Table 4) are for the uniform air distribution and different distributions of refrigerant. The capacity change as a result of calculated and imposed maldistributed refrigerant flows is insignificant for the uniform velocity profile for both R-22 and R-407C.

Table 5 shows refrigerant distribution, quality, and exit superheat for individual circuits. It is interesting to observe that for the UA-CR case the R-22 distribution is not uniform although all refrigerant circuits are identical. The difference in R-22 distribution is a consequence of different refrigerant superheats because of two causes. The first cause is related to the staggered tube arrangement and different airflow rates associated with circuit 1 and 6 (circuit 6 gets more airflow than circuit 1). The second cause is related to different tube-to-tube heat transfer via fins for circuit 1 and 6. The exit tube in circuit 1 is not directly exposed to the tubes from other circuits, while the exit tube of circuit 6 is directly exposed and exchanges heat with tube 5 of circuit 5. For R-407C, these effects apparently are compensated by R-407C temperature glide since distribution of R-407C is more uniform than that of R-22 in the UA-CR case.

The non-uniform air distribution notably affects capacity for both R-22 and R-407C even though the degree of its non-uniformity is not significant. For the case of maldistributed air and imposed uniform refrigerant distribution (MA-UR), the capacity ratio is equal to 0.91 for both refrigerants. For the simulated refrigerant distribution case (MA-CR), the capacity ratio for R-22 is 0.61 while for R-407C is 0.77, hence R-407C is less subject to air-flow maldistribution effects in the preferred cross-counter-flow configuration. One can note that a reduction in capacity corresponds to a reduction of refrigerant mass flow rate. This correspondence results from the same inlet quality and the same refrigerant superheat at the exit used in all simulations.

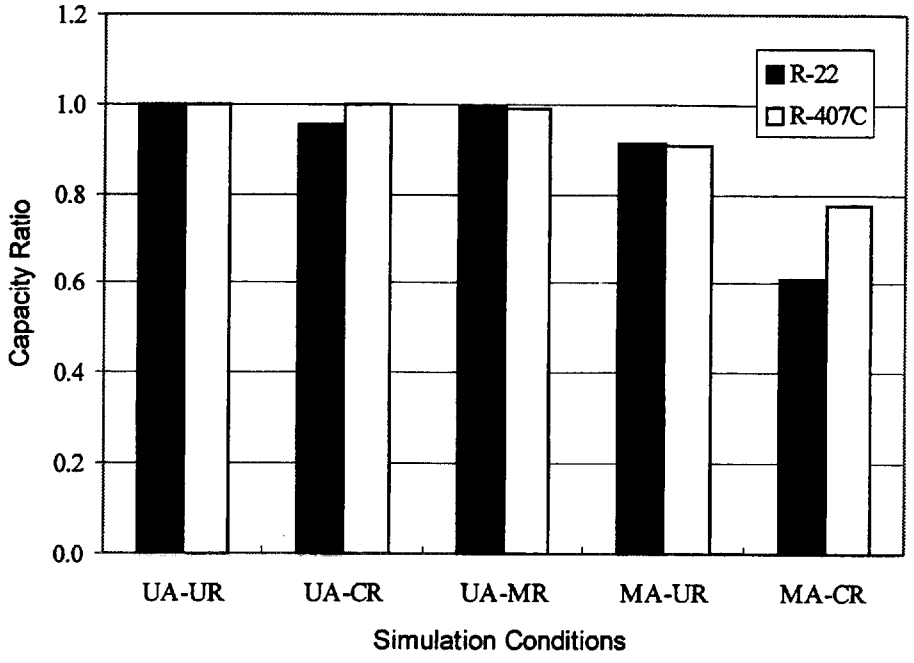

Figure 9. Ratio of capacities at different air and refrigerant distributions to the capacity at uniform air and refrigerant distribution for Coil A

Results for Coil B (parallel-cross-counter flow circuitry arrangement)

Figure 10 and positions 11 through 20 in Table 4 show relative capacity change for Coil B. The first three cases in Figure 10 (entries 11 through 13 and 16 through 18 in Table 4) are for a uniform air distribution with different distributions of refrigerant. Similarly to the cross-counter flow coil, degradation of coil capacity is insignificant for the studied distributions of refrigerant as long as the air velocity profile is uniform. For the imposed maldistributed air, the capacity degradation for R-22 and R-407C was similar, however, it varied with refrigerant distribution. For the uniform refrigerant distribution (MA-UR), the capacity ratio is 0.88 for both refrigerants. For the simulated refrigerant distribution (MA-CR), the capacity ratio for R-22 and R-407C is 0.65 and 0.73, respectively.

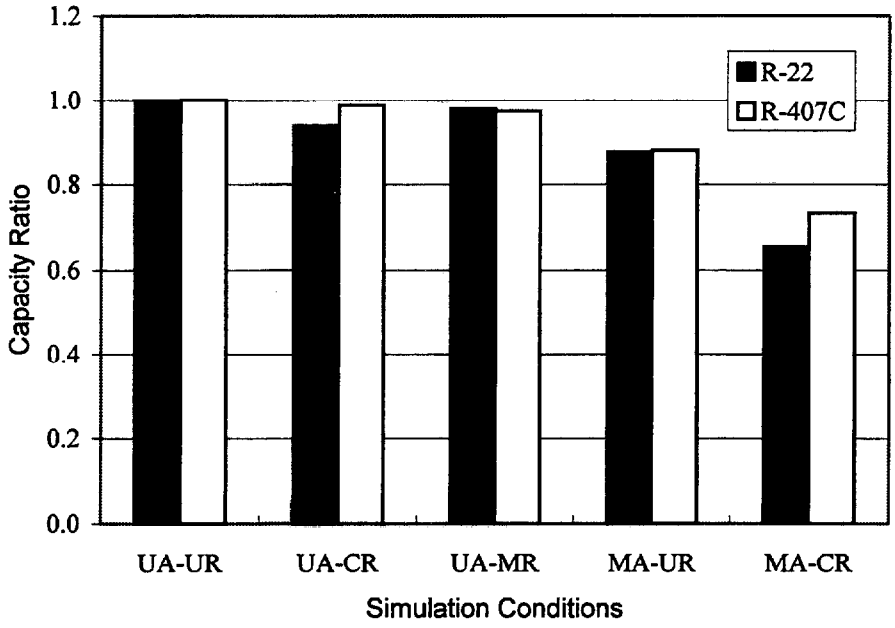

Figure 10. Ratio of capacities at different air and refrigerant distributions to the capacity at uniform air and refrigerant distribution for Coil B

Results for Coil C (cross-flow circuitry arrangement)

Figure 11 and positions 21 through 30 in Table 4 show relative capacity change for Coil C. The first three cases in Figure 11 (entries 21 through 23 and 26 through 28 in Table 4) are for uniform air distribution. A small degradation in coil capacity was observed with the uniform velocity profile and calculated refrigerant distribution, 8% and 2% for R-22 and R-407C, respectively. All three non-uniform velocity profiles (MA1-CR, MA2-CR, and MA3-CR) caused significant capacity degradation. It is interesting to notice that for a given refrigerant the capacity penalties for these three cases are similar, with the penalties for R-407C being larger than that for R-22. The degradation of capacity is related to maldistribution of refrigerant between different circuits shown in Table 5.

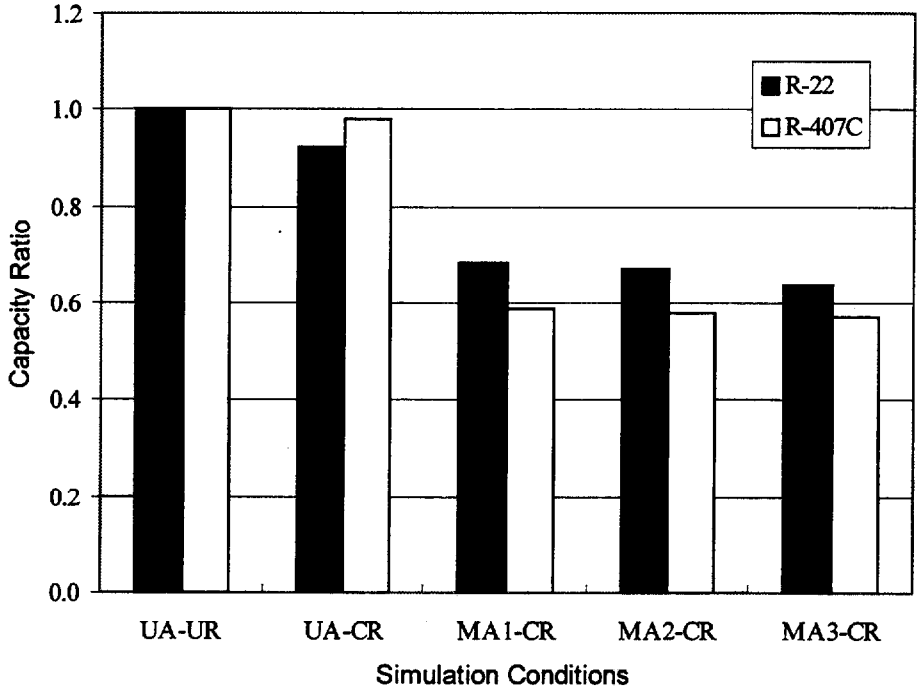

Figure 11. Ratio of capacities at different air and refrigerant distributions to the capacity at uniform air and refrigerant distribution for Coil C

CONCLUDING COMMENTS

Simulation results showed that R-22 and R-407C have similar susceptibility to capacity degradation. Capacity degradation may be smaller for R-22 or for R-407C depending on the air velocity profile and refrigerant circuitry design. Therefore, this study cannot recommend a general rule for estimating a capacity degradation for R-22 and R-407C, since each combination of coil design and fluid distribution has to be evaluated case by case. For the cross-counter-flow configuration (best suited to R-407C from a system perspective), R-407C showed less capacity loss for the air-flow maldistributions studied.

For the cases studied, the results showed a much greater sensitivity to air maldistribution than to refrigerant maldistribution. For Coil A and Coil B where simulations with maldistributed air were performed for uniform and calculated refrigerant distributions, the results for the latter case showed a more significant capacity degradation. This indicates that maldistributed air affected refrigerant distribution, which caused a further degradation of the simulated coil capacity.

A note has to be made regarding the simulation program, EVAP5M. The new feature of EVAP5M, the algorithm accounting for heat transfer between neighboring tubes via fins, was only partially verified because of the limited scope of this project. However, this validation warranted the inclusion of this algorithm into the simulation scheme. The assumptions accepted in the algorithm (including those for shape factors) should not affect the final conclusions of this report since all results are considered on a relative basis.

EVAP5M would benefit from improved heat transfer and pressure drop correlations. On the air side, the air distribution for case MA3-CR (Coil C) assigned close to zero air velocities for the bottom and top tubes in the evaporator assembly. These velocities resulted in a low value of the Reynolds number, which was below the lower limit for which the air-side heat-transfer correlation was developed. On the refrigerant side, the available pressure drop and heat transfer correlations for micro-finned tubes are far from satisfactory. For this reason the results of this study have been presented on a relative basis. This approach offers more validity and should generate sufficient confidence for practical engineering purposes.

REFERENCES

1. Domanski, P.A., EVSIM-An Evaporator Simulation Model Accounting for Refrigerant and One Dimensional Air Distribution, NISTIR 89-4133, National Institute of Standards and Technology, Gaithersburg, MD, 1989.
2. Domanski, P.A., Simulation of an Evaporator with Nonuniform One Dimensional Velocity Distribution, *ASHRAE Transactions*, Paper No. NY-91-13-1, Vol. 97, Part 1, 1991.
3. Kays, W.M., and London, A.L., Compact Heat Exchanger, McGraw-Hill, 1984.
4. Gallagher, J., McLinden, M.O., Morrison, G., and Huber, M., NIST Standard Reference Database 23, Version 5.0 (REFPROP), National Institute of Standards and Technology, Gaithersburg, MD, 1993.
5. Martys, N., private communication, National Institute of Standards and Technology, Gaithersburg, MD, November 1996.
6. Gray, D.L., and Webb, R.L., Heat Transfer and Friction Correlations for Plate Finned-Tube Heat Exchangers Having Plain Fins, *Proc. of Eighth Int. Heat Transfer Conference*, San Francisco, 1986.
7. Webb, R.L., Air-Side Heat Transfer Correlation for Flat and Wavy Plate Fin-and-Tube Geometries, *ASHRAE Transactions*, Paper No. SL-90-1-2, Vol. 96, Part 2, 1990.
8. Nakayama, W., and Xu, L.P., Enhanced Fins for Air-Cooled Heat Exchangers Heat Transfer and Friction Factor Correlations, *Proceedings of ASME-JSME Thermal Engineering Joint Conference*, P.495, March 1983, ASME, New York, 1983.
9. McQuiston, F.C., and Parker, J.D, Heating, Ventilating, and Air Conditioning, J.Wiley & Sons, 1982.
10. Sheffield, J.W., Wood, R.A., and Sauer, H.J., Experimental Investigation of Thermal Conductance of Finned Tube Contacts, *Experimental Thermal and Fluid Science*, Elsevier Science Publishing Co., Inc., New York, NY, 1988.
11. American Society of Heating, Refrigerating and Air conditioning Engineers, Inc. ASHRAE Handbook, Fundamental Volume, New York, 1993.
12. Jung, D.S., and Didion, D.A., Horizontal Flow Boiling Heat Transfer using Refrigerant Mixtures, ER-6364, EPRI Project 8006-2, May 1989.
13. Petukhov, B.S., Heat transfer and friction in turbulent pipe flow with variable physical properties, *Advances in Heat Transfer*, Vol. 6., pp. 503-564, Academic Press, New York, 1970.
14. Pierre, B., Flow Resistance with Boiling Refrigerants, *ASHRAE Journal*, September 1964.
15. Schlichting, H., Boundary-Layer Theory, Sixth Edition, McGraw-Hill, Inc., 1968.
16. Bergles, A.E., Collier, J.G., Delhaye, J.M., Hewitt, G.F., and Mayinger, F., Two-Phase Flow and Heat Transfer in the Power and Process Industries, Hemisphere Publishing Corp., New York, NY, 1981.
17. Schlager, L.M., Pate, M.B., and Bergles, A.E., Heat Transfer and Pressure Drop during Evaporation and Condensation of R-22 in Horizontal Micro-fin Tubes, *Int. J. Refrig.*, Vol. 12, No. 1, 1989.

APPENDIX A. USER'S MANUAL FOR EVAP5M

EVAP5M predicts the performance of a finned-tube evaporator operating with R-22 and R-407C. The model can account for one-dimensional maldistribution of air at the evaporator inlet. The simulation results include total and latent capacity, outlet refrigerant and air parameters, including refrigerant parameters at the outlet of individual circuitry branches. This appendix explains the input data to the program and presents an example run with simulation results.

Input Data

The input to the program consists of the following information:

- evaporator design data
- refrigerant selection
- operating conditions

Evaporator design data has to be coded in a data file in the format presented in Table A1. The default name for the evaporator file is EVONLY.INP. EVAP5M reads this file automatically when it enters "Evaporator Menu." The user can also use an evaporator data file with an arbitrary name and instruct EVAP5M to read this file. Table A2 shows an example of the evaporator data file. Figure A1 shows basic evaporator dimensions and specification of circuitry.

Refrigerant selection between R-22 and R-407C is done interactively. Based on the user's selection, refrigerant properties can be calculated using either REFPROP [4] subroutines or the refrigerant property look-up tables supplied with the program.

Operating conditions can be either coded in a data file or can be specified interactively from the "Operating Conditions Menu." The name of the default data file is EVOP.INP, but any arbitrary name can also be assigned. Table A3 contains an example of a file with operating conditions. Figure A2 shows an example of air velocity profile.

Example Simulation Run

Starting with the opening screen displayed in Figure A3, five figures show the main interaction screens of EVAP5M. Figure A4 shows the Main Menu screen. The program starts with R-22 as the selected refrigerant. The user may switch to R-407C by choosing option 3. For faster simulation, it is suggested to load the look-up table (option 4) before proceeding to the Evaporator Menu (option 1). If the look-up table is not loaded, EVAP5M uses REFPROP subroutines directly to calculate all thermophysical properties.

Figure A5 shows the Evaporator Menu screen. With this menu coming on the screen, EVAP5M loads the default evaporator data file EVONLY.INP. The user may specify another evaporator data file by choosing option 2. The first line of the evaporator data file is displayed as "Current Coil ID." Choose option 3 to proceed to the "Operating Conditions Menu."

Figure A5 shows the options available in the "Operating Conditions Menu." The user has to provide EVAP5M with operating conditions by choosing option 1, 2 , or 3. Up to this point, the user prepared necessary data files for EVAP5M and provided the program with execution instructions. Selecting option 5 will finally start the evaporator simulation.

Table A4 presents simulations results for R-407C. These results were obtained for the evaporator described in Table A2 at the operating conditions specified in Table A3. A look-up table was used for calculating thermophysical properties. When a simulation run is completed and results displayed, the program returns to the menu shown in Figure A7. Option 4 allows for saving the simulation results in a user-named file. The user may exit EVAP5M via the Main Menu (option 0) or perform the next simulation run with different operating conditions or a different heat exchanger.

Table A1. Format for evaporator data file

All input data are in FORTRAN free field input format with data values on the same lines separated by commas. The standard FORTRAN convention for Real and Integer variables applies.

Line 1: COILID
COILID = alphanumeric coil information, maximum 70 characters

Line 2: NSLABS
NSLABS = number of heat exchanger slabs in the coil assembly

Line 3: NDEPTH, NTUBE
NDEPTH = number of heat exchanger slabs in the coil assembly
NTUBE = number of tubes in one slab

Line 4: DI , DO, TPCH, DPCH, WIDTH, BSIDE, BSPACE (see Figure A1)
DI = tube inside diameter, for grooved tubes use the minimum diameter (mm)
DO = tube outside diameter (mm)
TPCH = tube pitch in each depth row (mm)
DPCH = distance between neighboring tube depth rows (mm)
WIDTH = width of a coil, equal to the length of tubes to the duct air (mm)
BSIDE = height of the coil (mm)
BSPACE = distance between the edge of the coil and location of tube # 1 (mm)

Line 5: FPCH, FTK, FMK, TMK
FPCH = center to center distance between fins (mm)
FTK = fin thickness (mm)
FMK = fin material thermal conductivity (kW/(m·K))
TMK = thermal conductivity of a tube material (kW/(m·K))

Line 6: IFIN, ISUR, ENH1, ENH2
IFIN = 1 for flat fins
= 2 for wavy fins
= 3 for lanced fins
ISUR = 1 for a smooth inner surface
= 2 reserved for a smooth tube with a twisted tape insert
= 3 for rifled tubes
ENH1 = tape twist ratio for ISUR = 2
For ISUR=1 or 3, ENH1=0.0
ENH2 = tape thickness for ISUR = 2
For ISUR=1 or 3, ENH1=0.0

Line 7: NSECT
NSECT = number of repeating sections in a given slab

Line 8: NTUB(1), NTUB(2), NTUB(3), NTUB(4), NTUB(5)
NTUB(1) = number of tubes in the first depth row in a section (facing the incoming air)
NTUB(2) = number of tubes in the second depth row in a section
NTUB(3) = number of tubes in the third depth row in a section
NTUB(4) = number of tubes in the fourth depth row in a section
NTUB(5) = number of tubes in the fifth depth row in a section

Line 9: IFROM(I), I = 1,10 (See Figure A1 and Table A2 for an example of circuitry specification. Use the number 999 for a nonexistent tube. Use the number 0 to designate the inlet tube to the evaporator.)

IFROM(1) = number of the tube from which tube 1 receives refrigerant
IFROM(2) = number of the tube from which tube 2 receives refrigerant
IFROM(3)
.
.
IFROM(9)
IFROM(10)= number of the tube from which tube 10 receives refrigerant

Line 10: IFROM(I), I = 11,20

IFROM(11) = number of the tube from which tube 11 receives refrigerant
IFROM(12) = number of the tube from which tube 12 receives refrigerant
IFROM(13)
.
.
IFROM(19)
IFROM(20)= number of the tube from which tube 20 receives refrigerant

Line 11: IFROM(I), I = 21,30

Line 12: IFROM(I), I = 31,40

Line 13: IFROM(I), I = 41,50

Line 14: IFROM(I), I = 51,60

Line 15: IFROM(I), I = 61,70

Line 16: IFROM(I), I = 71,80

Line 17: IFROM(I), I = 81,90

Line 18: IFROM(I), I = 91,100

Line 19: IFROM(I), I = 101,110

Line 20: IFROM(I), I = 111,120

Line 21: IFROM(I), I = 121,130

Line 22: NTEST(1) (See Figure A2 and Table A2 for the explanation of air velocity profile coding.)

NTEST(1) = number of air velocity measurement points;
possible values: minimum 1, maximum 16

Line 23: X(N), N=1,8

X(1) = location of the first air velocity measurement point
(distance between the edge of the slab closest to tube #1 and the velocity measuring probe) see Figure (A3) (mm)
X(2) = location of the second air velocity measurement point
X(3) = location of the third air velocity measurement point; if non-existent, input 0.0 (mm)
.
.
X(8) = location of the eighth air velocity measurement point; if non-existent, input 0.0 (mm)

Line 24: X(N), N=9,16

X(9) = location of the ninth air velocity measurement point; if non-existent, input 0.0 (mm)
X(10)
.
.
X(16) = location of the sixteenth air velocity measurement point; if non-existent, input 0.0 (mm)

Line 25: VX(N), N=1,8
VX(1) = air velocity at the first measurement point (m/s)
VX(2) = air velocity at the second measurement point (m/s)
VX(3) = air velocity at the third measurement point; if non-existent, input 0.0 (m/s)
.
.
VX(8) = air velocity at the eighth measurement point; if non-existent, input 0.0 (m/s)

Line 26: VX(N), N=9,16
VX(9) = air velocity at the ninth measurement point (m/s)
VX(10)
.
.
VX(16) = air velocity at the eighth measurement point; if non-existent, input 0.0 (m/s)

Table A2. Example of a data file for a one-slab evaporator
(This file codes the refrigerant circuitry and velocity profile shown in Figure A2)

```
AN EXAMPLE EVAPORATOR (any text)
1
3,16
9.220,10.01,25.4,22.23,454.0,408.0,20.64
2.004,0.2032,0.2216,0.3860
2,1,0.,0.
1
16,16,16,0,0
2,3,19,5,6,22,23,7,8,25
10,27,12,30,14,15,33,17,18,4
37,21,39,0,9,11,28,45,13,31
32,48,34,35,36,20,38,41,40,24
42,25,26,43,44,29,46,47,999,999
999,999,999,999,999,999,999,999,999,999
999,999,999,999,999,999,999,999,999,999
999,999,999,999,999,999,999,999,999,999
999,999,999,999,999,999,999,999,999,999
999,999,999,999,999,999,999,999,999,999
999,999,999,999,999,999,999,999,999,999
999,999,999,999,999,999,999,999,999,999
999,999,999,999,999,999,999,999,999,999
6
25.0, 100.0, 165.1, 245.0, 285.0,345.0,0., 0.
0., 0., 0., 0., 0., 0., 0.,0.
1.35, 1.72, 1.5, 1.0, 1.35, 1.1, 0.,0.
0., 0., 0., 0., 0., 0., 0., 0.
```

Table A3. Example of a data file with evaporator operating conditions

```
Operating conditions, example (any text)
Refrig. inlet pressure (kPa)    ,670.
Refrig. inlet quality (-)       ,0.2
Refrig. mass flow rate (kg/h)   ,90.
Air inlet temperature (C)       ,26.7
Air inlet pressure (kPa)        ,101.325
Air inlet relative humidity (-),0.5
Air mass flow rate (kg/h)       ,1000.
Fan power (kW)                  ,0.0
```

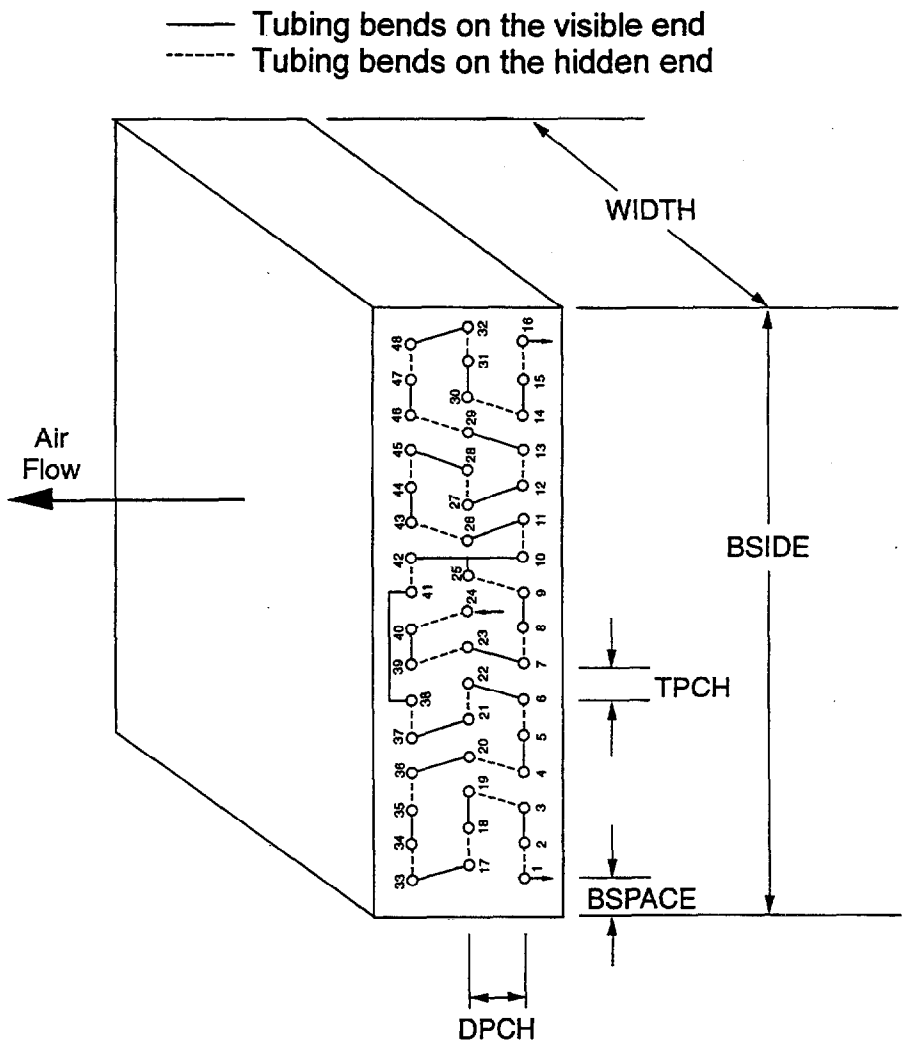

Figure A1. Specification of evaporator circuitry and dimensions

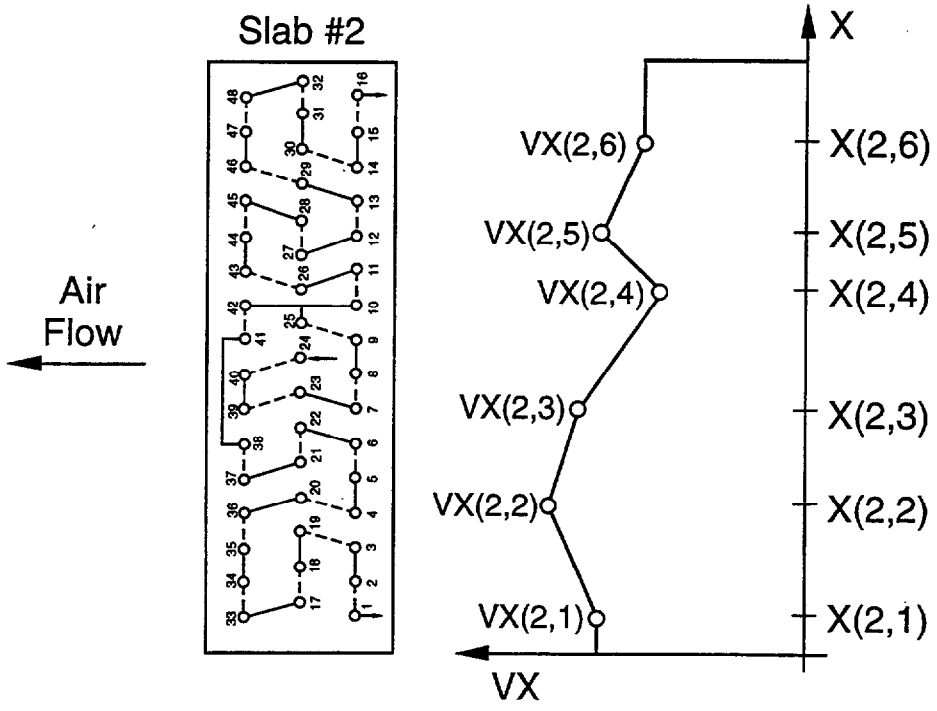

Figure A2. Example of air velocity measurement points and velocity profile

Table A4. Example of simulation results

```
------------------EVAP5M SIMULATION SUMMARY-------------------

 Coil ID: AN EXAMPLE EVAPORATOR DATA FILE (any text)
 Refrigerant:          R32     R125    R134a
 Weight Composition:   0.230   0.250   0.520

 REFRIGERANT SIDE
 Refrigerant mass flow rate:              90.0    [kg/h]
 Sensible capacity:                        3.197  [kW]
 Latent capacity:                          1.059  [kW]
 Total capacity:                           4.256  [kW]
 Outlet saturated temp. and superheat:    10.0      1.3   [C]
 Inlet and outlet temperatures:            6.3     11.4   [C]
 Inlet and outlet pressures:             670.0    644.2   [kPa]
 Inlet and outlet qualities:               0.200   1.000

 AIR SIDE
 Air mass flow rate:                    1000.0    [kg/h]
 Air-side capacity (with fan):             4.256  [kW]
 Fan power:                                0.000  [kW]
 Air temperature (downstream the fan):    15.9    [C]
 Air temperature distribution [C]:        26.7  20.9  18.6  15.9
 Air humidity    distribution [%]:        .5000 .6836 .7387 .8343

 CONDITION OF REFRIGERANT LEAVING OUTLET TUBES
 Tube      Quality     Temperature     Superheat
   #         (-)           (C)            (C)

   1       1.000          20.4           10.4
  16       0.974           9.9            0.0
```

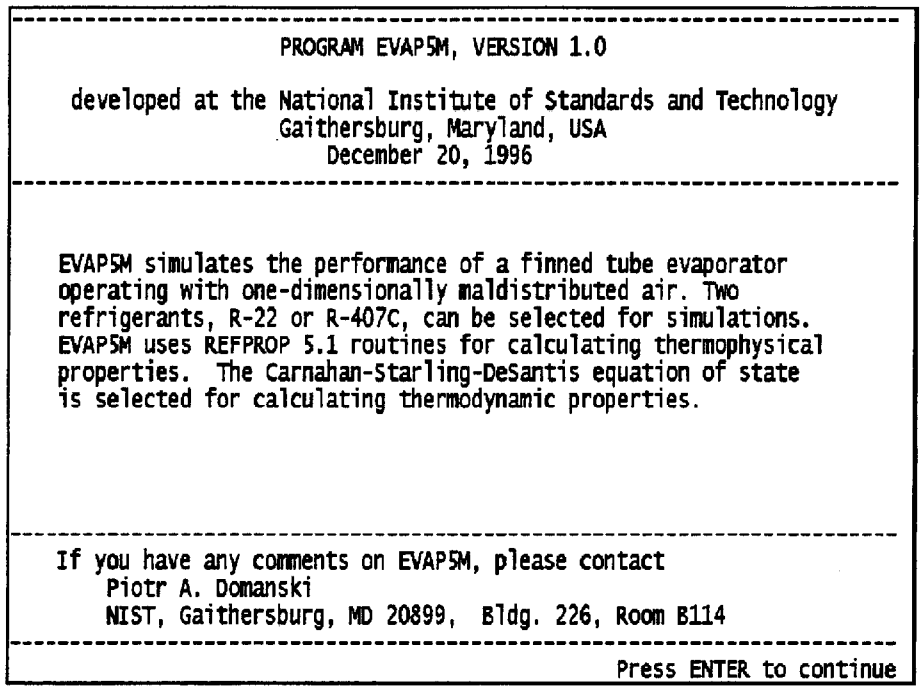

Figure A3. Opening screen of EVAP5M

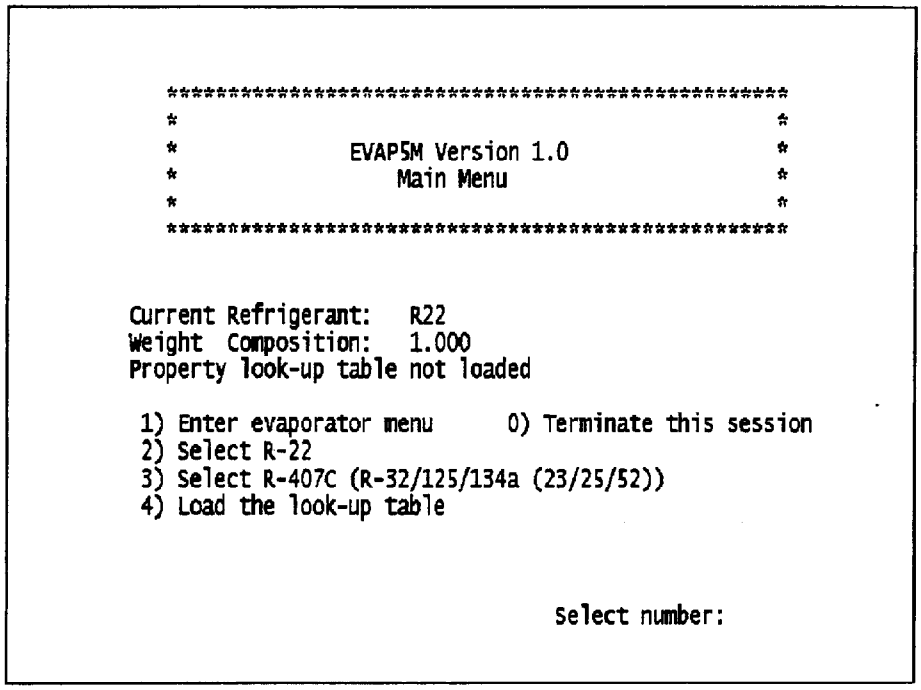

Figure A4. Main Menu screen

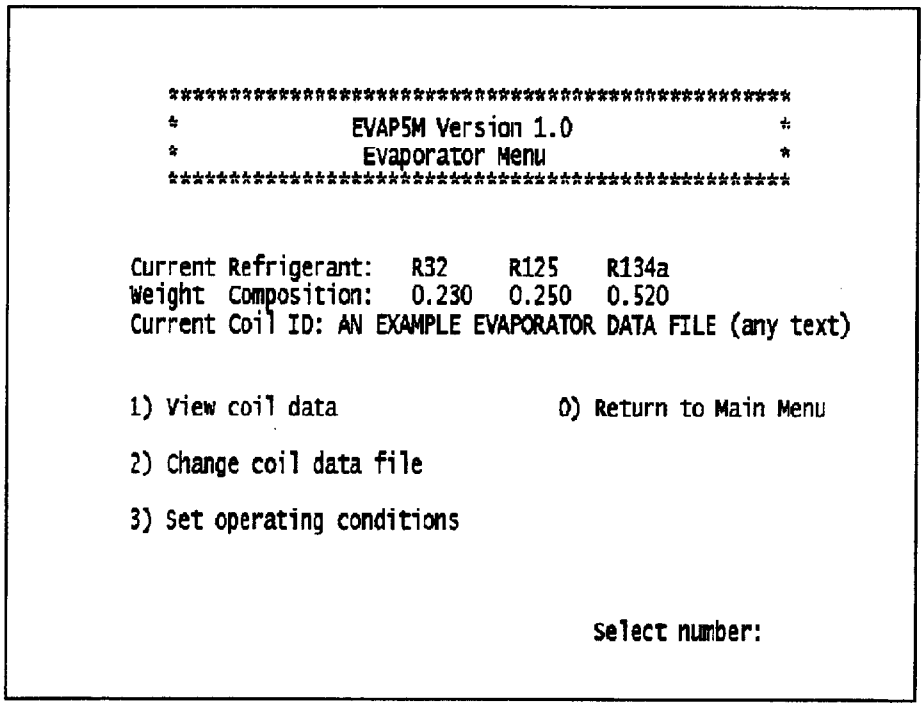

Figure A5. Evaporator Menu screen before simulation

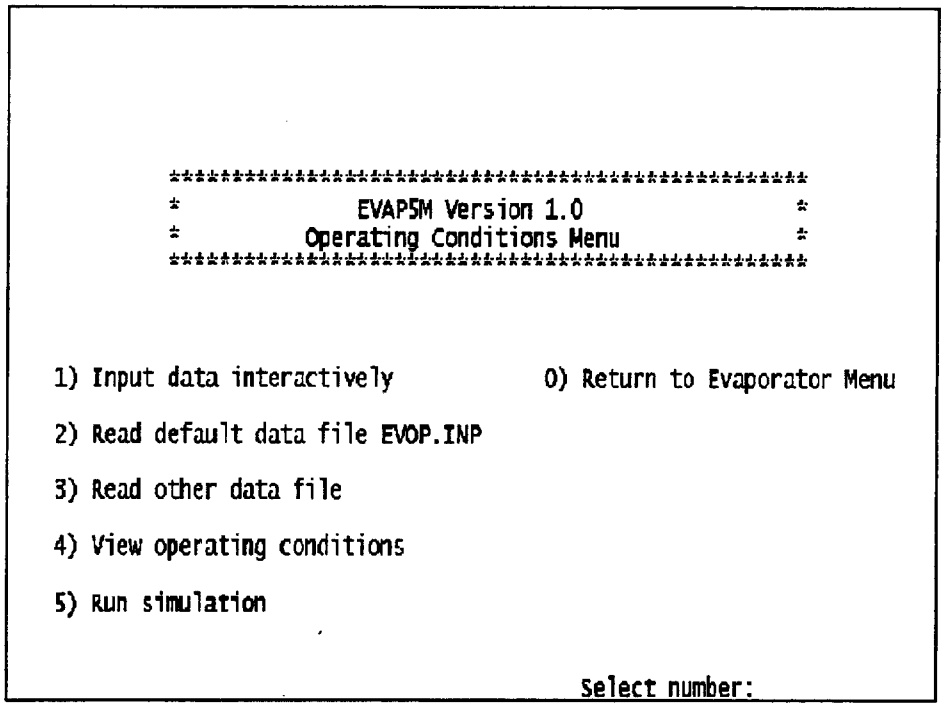

Figure A6. Operating Conditions Menu screen

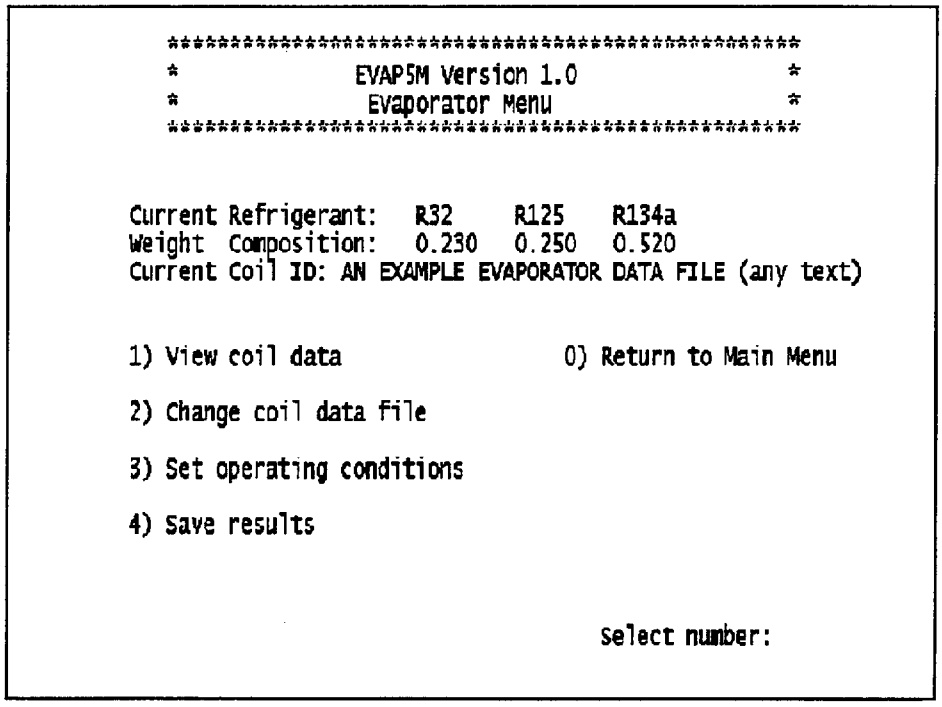

Figure A7. Operating Conditions Menu after simulation